Available online at www.sciencedirect.com
ScienceDirect
Acta Materialia 57 (2009) 4032–4035
Acta MATERIALIA
www.elsevier.com/locate/actamat

Nanomechanics of rhenium wires: Elastic modulus, yield strength and strain hardening

L. Philippe [a,*], Z. Wang [a], I. Peyrot [a], A.W. Hassel [b], J. Michler [a]

[a] EMPA (Swiss Federal Laboratories for Materials Testing and Research), Feuerwerkerstrasse 39, 3602 Thun, Switzerland
[b] Max-Planck Institute für Eisenforschung, Max-Planck-Strasse 1, D-40237 Düsseldorf, Germany

Received 9 February 2009; received in revised form 22 April 2009; accepted 24 April 2009
Available online 17 June 2009

Abstract

We report on the mechanical properties of rhenium wires that range in diameter from 400 to 1000 nm under bending, using in situ atomic force microscopy measurements inside a scanning electron microscope combined with finite-element simulations. Load–displacement curves are obtained from elastoplastic bending of nanowires. The average values of the bending modulus and yield stress of nanowires are found to be about 437 and 25 GPa, respectively. Computational simulations have been carried out to fit a power-law strain-hardening model to the experimental load–displacement curves. This allowed the true stress–strain curves to be reconstructed for simple bending experiments.

Keywords: Rhenium nanowires; Elasticity; Plasticity; Modeling

1. Introduction

Rhenium nanowires (RhNWs) are unique nanoscale materials that exhibit high strength and interesting electric properties. Their hexagonal atomic structures also give them particular mechanical properties [1], which are different from those of face-centered cubic structures such as Au or Ag nanowires. These properties could make them ideal for technological applications in electromechanical sensors, field emission devices, scanning probe microscopes and interconnects [2–5]. Characterizing the mechanical properties of nanowires is therefore of great importance in view of their future applications.

The mechanical properties of nanomaterials have long been known to change with the amount of probed volume at the micro/nanoscale [6–10]. The mechanisms that govern small-scale plasticity in metals are generally related to dislocation storage, motion, pinning and nucleation over the submillimeter to nanometer scale [11]. Unlike silicon or germanium nanowires [12], to the best of our knowledge, the elastoplastic properties including the strain-hardening behavior of RhNWs, have not yet been investigated. In an earlier paper [13], the mechanical properties of a hexagonal crystal structure have been evaluated for the first time for monocrystalline RhNWs. Numerical and analytical findings reported yield stress values of around 26 GPa for RhNW, which represents almost 10% of the Young's modulus value and 100 times higher than the yield stress reported for its bulk counterpart. Discrepancies and errors intrinsic to the experimental data clearly underlined the importance of an advanced numerical model to measure accurately the yield stress of RhNWs. The effects of substrate, stiffness anisotropy and surface state properties of the system were investigated, and it was shown that their influence on the resulting mechanical properties cannot be neglected.

The measurement on free-standing nanowires is always challenging since the mechanical properties determined by standard macroscale materials testing procedures cannot easily be employed for nanomaterials. Several methods have been reported for measuring the mechanical

* Corresponding author. Fax: +41 33 228 44 90.
E-mail address: Laetitia.Philippe@empa.ch (L. Philippe).

1359-6454/$36.00
doi:10.1016/j.actamat.2009.04.047

properties of nanowires, including resonance [9,14,15] and cantilever bending [16,13] methods. In this article, we present an in situ atomic force microscopy (AFM) method combined with an inverse finite-element (FE) analysis to determine the mechanical properties of free-standing RhNWs under large strain. The bending modulus and the ultimate stress are measured using a nanobending experiment. Experimental data is then analyzed using FE simulations to calculate the strain-hardening coefficient. The combination of experiment and theoretical simulation yields a complete analytical elastoplastic model for the analysis of the stress–strain behavior.

2. Nanobending experiments

In our experiments, we use monocrystalline RhNWs, which are synthesized by directional solidification of an eutectic NiAl–Rh alloy and subsequent selective etching of the NiAl matrix [17]. To carry out the nanobending experiment, a rectangular AFM cantilever fixed at one end on a nanomanipulation system was set up inside a chamber of scanning electron microscope (SEM), as reported in detail elsewhere [13]. The AFM tip has been used to apply a lateral force on the wire tip to bend individual free-standing RhNWs embedded into NiAl substrate.

In order to avoid possible sliding between the AFM tip and nanowires, a contamination deposit was realized. We used a focused ion beam to decompose hydrocarbon molecules from the sample surface present in the SEM chamber at a pressure of 10^{-6} mbar to form this joint deposit on the AFM tip.

Fig. 1 shows SEM images of a RhNW during bending and after bending; different stages of deformation are demonstrated. As noted in this figure, the displacement δ is obtained directly from the displacement of the RhNW through image analysis during the bending test. The load (lateral force) F is measured by combining the displacement of the tip and the transverse spring constant K_c^t of the tip ($F = K_t\delta_c$, where δ_c is the displacement of the cantilever tip). The AFM cantilever exhibits a calibrated normal spring constant K_c^n between 0.2 and 0.75 N m^{-1}. The following equation gives the exact value of the transverse force constant K_t:

$$K_c^t = \frac{3E_cI}{l_c^3} = \frac{E_c w_c t_c^3}{4l_c^3} \quad (1)$$

where the subscript c indicates the cantilever, E_c is the bending modulus of the cantilever, and l_c, t_c and w_c are its length, thickness and width, respectively. The bending modulus of the cantilever is $E_c^t = 169$ GPa in the longitudinal $\langle 1\,1\,0\rangle$ direction [19]. The dimension of the AFM tip and the cantilever is measured from high-resolution SEM imaging. The calculated transverse spring constant is about 19.72 N m^{-1}.

3. Results

In this study, the elastoplastic parameters of RhNWs were obtained from the analysis of F–δ (force–displacement) curves. One example is shown in Fig. 2. This curve is typical for a material exhibiting elastoplastic behavior. The initial linear slope corresponds to the elastic region. A breakdown of the linear load–displacement slope corresponds to the initiation of plastic deformation observed by in situ image analysis. Finally, strain localization on the wire takes place, corresponding to changes in the area of the cross-section. The mechanism of this is still not clear and the observed transition from strain hardening to strain softening does not always correspond to the observed strain localization of nanowires as shown in Fig. 1c. In the following, we analyze the F–δ curves of each bent nanowire to obtain the values of their bending modulus E and yield stress σ_y.

In the elastic region, the bending modulus E of RhNWs is calculated using the Euler–Bernoulli isotropic beam

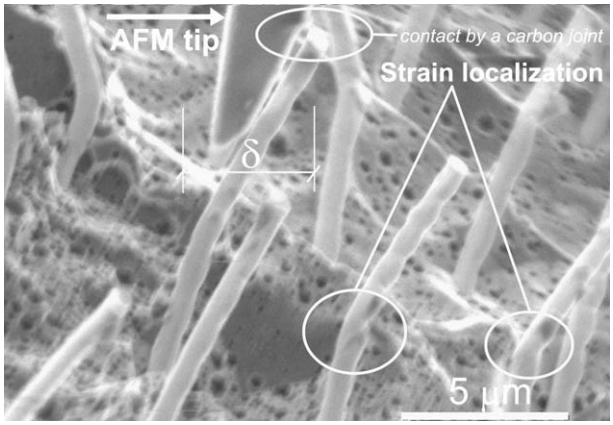

Fig. 1. SEM image of RhNWs during a bending experiment. A real-time movie of this nanomanipulation is available as Supplementary material [18].

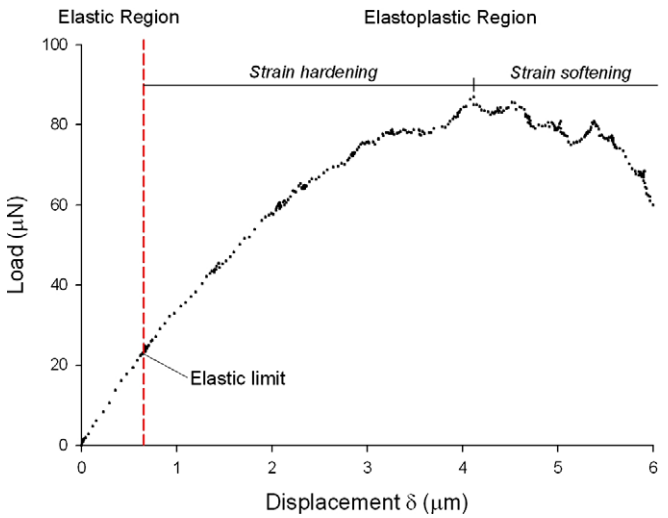

Fig. 2. Example of F–δ curve obtained from the nanobending experiment on a RhNW. The elastic and elastoplastic regions are separately labeled on the curve.

theory, in which the relationship between the displacement, the force and the bending modulus without friction can be written as:

$$EI\frac{d^4\delta}{dy^4} = F \tag{2}$$

where I is the area moment of inertia of the wire with $I = \omega^4/12$ if we assume a square cross section [13], δ is the tip displacement. The lateral force F is applied in y direction. From this differential equation, E can be calculated as follows:

$$E = \frac{FL^3}{3I\delta} \tag{3}$$

Error sources that are intrinsic to the dimension measurements used for solving Eq. (3) are estimated to be at most 15% for the width w, the length L of the RhNW and the measured displacement δ (for details see Ref. [13]). We consider also a maximum error of 5% for the width w_c, length l_c and thickness t_c of the AFM cantilever, as its dimensions were characterized prior to bending experiments using a high-resolution SEM. The relative experimental error $(\triangle E/E)$ can be written as:

$$\frac{\Delta E}{E} = 3\left|\frac{\Delta w_c}{w_c}\right| + \left|\frac{\Delta t_c}{t_c}\right| + 3\left|\frac{\Delta l_c}{l_c}\right| + 3\left|\frac{\Delta L}{L}\right| + 4\left|\frac{\Delta w}{w}\right| \tag{4}$$

By taking into account the imprecision in the measurement of the dimensions, the estimated maximum error in the Young's modulus is approximately ±170%. However, the errors from fixation is difficult to estimate since the substrate surface is not totally planar and the clamping depth of the nanowire into the substrate is unknown.

We plot the measured bending moduli E in Fig. 3. A surprisingly good agreement has been achieved between our average value 437 GPa and the theoretical one of Re in the growth direction $\langle\bar{2}023\rangle(472 \pm 25\ \text{GPa})$.

The F–δ curves (e.g. Fig. 2) show the plastic deformation of RhNWs during bending and several load drops. One possible explanation is the nucleation of dislocations that propagate across the nanowire and then partly exit the wire at the other end. It is possible to evaluate yield stress σ_y values of the RhNWs from these curves. Here, σ_y was calculated by means of an inverse method using FE simulations [26]. In the literature, there are many reported mechanical measurements of yield stress of micro- and nanostructures, though with widely varying results. The main mechanisms in metals are size-dependent dislocation storage, multiplication, motion, pinning and nucleation [10,20].

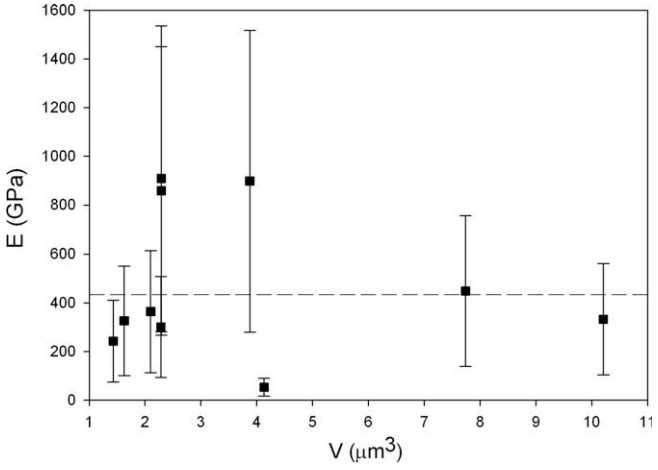

Fig. 3. Experimental bending modulus values obtained from F–δ curves for 10 RhNWs vs. aspect ratio L/w. Dashed line shows the average value 437 GPa. Error bars stand for maximum error estimation: 170%.

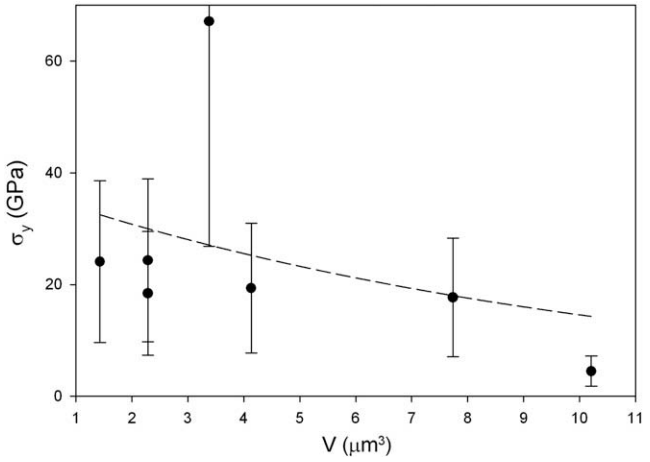

Fig. 4. σ_y values obtained from bending experiments for seven RhNWs as a function of $V = Lw^2$. The dashed line is a fitted curve for visual guidance only. The average value is about 25 GPa. The estimated maximum error in the yield stress is about 60% [13].

We plot σ_y as a function of the wire volume $V = L \times w^2$ in Fig. 4. It seems that σ_y decreases with the size of wire. This size dependence may be qualitatively comparable with that found for gold nanowires [21,11] and Ni_3Al–Ta microstructures [10]. We can therefore conclude that the smaller the wires get, the stronger they are. The average value of σ_y that we obtain here is about 25.1 GPa, which is in agreement with values recently reported in the literature [13]. Moreover, the present experimental methods provide an efficient means to record F–δ curves for mechanical events on nanowires.

4. Modeling

In order to build a constitutive law for the elastoplastic behavior of RhNWs, we analyzed our experimental data using an inverse method, which consists in fitting mechanical properties parameters to sets of experimental results. From classical theories of plasticity, we use the power-law work-hardening model [22], which is considered as a fairly good approximation for metals. In this model, the relationship between the true stress σ and the true strain ϵ can be written as follows:

$$\sigma = \begin{cases} E\epsilon & \text{if } \sigma \leqslant \sigma_y \\ \sigma_y\left(1 + \frac{E\epsilon^p}{\sigma_y}\right)^n & \text{if } \sigma > \sigma_y \end{cases} \tag{5}$$

where n is the strain-hardening exponent, ϵ^p is the plastic strain and ϵ is the total strain. The von Mises yield criterion is assumed.

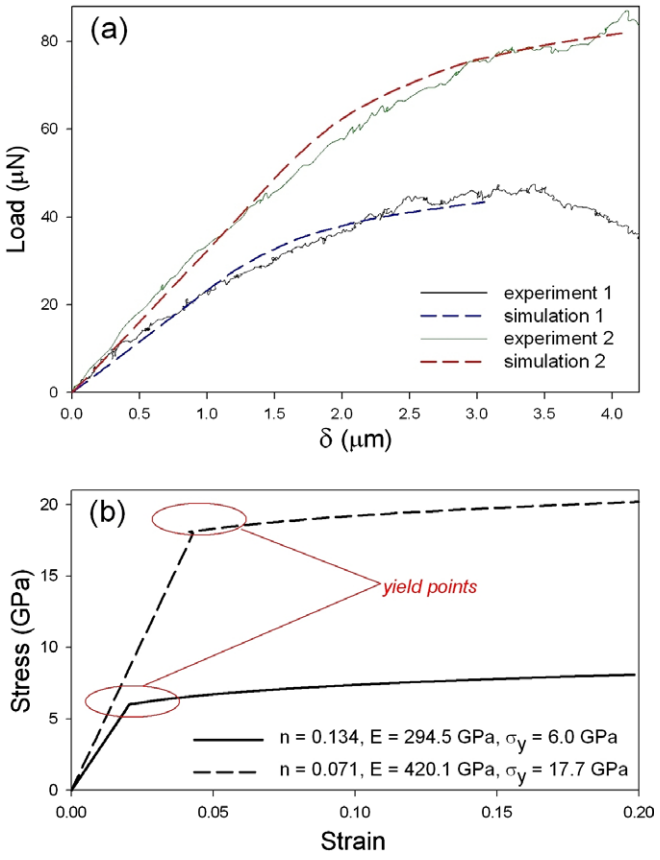

Fig. 5. (a) Comparison of experimental F–δ curves with those from FE simulation. (b) Reconstructed true stress–strain curves for these two RhNWs.

Three-dimensional isotropic FE simulations have been carried out to fit the elastoplastic hardening model [23]. A mesh of quadrilateral elements has been built for the whole system. A bilateral sticking contact between the tip and the RhNW is assumed. Convergence studies have been carried out to ensure the validity of simulation results.

Different values of the strain-hardening exponent n are used in the simulation to fit experimental F–δ curves. It is shown in Fig. 5a that the the power-law strain-hardening model gives a good description to the elastoplastic behavior of RhNWs before the plastic instability (strain softening) occurs. The values of n found by the calculation are in the range 0.071–0.134. We note that the decreasing part of the F–δ curves (strain softening part) cannot be fitted by the classical strain-hardening model as the FE model always predicts a homogeneous deformation of the wire [24]. In Fig. 5c, stress–strain curves have been reconstructed based on the best fit of E, σ_y and n for the load–displacement curves achieved experimentally. We can see that RhNWs exhibit almost ideal plastic behavior, since the average hardening rates of RhNWs are quiet small (tangent modulus θ/E ranging from 0.03 to 0.09). Hence we can conclude that the plastic instability of RhNWs mainly depends on the value of yield stress [25].

In summary, we have investigated elastoplastic properties of RhNWs under large strain, using the combination of AFM bending experiments and numerical analysis. The yield stresses of RhNWs are found to decrease with increasing wire size. In our inverse analysis, numerical simulations have been carried out to give a complete description of the elastoplasticity of the nanowires. The power-law strain-hardening model has been found to give an accurate description of the elastoplastic behaviors of RhNWs.

Acknowledgements

Financial support by the Swiss State Secretariat for Education and Research in the frame of the European Project HYDROMEL (under contract No. 026622-2) is gratefully acknowledged. We thank M. Zaiser at the University of Edinburgh for helpful discussions.

Appendix A. Supplementary material

Supplementary data associated with this article can be found, in the online version, at doi:10.1016/j.actamat.2009.04.047.

References

[1] Qian D, Wagner G, Liu W, Yu MF, Ruoff R. Appl Mech Rev 2002;55:495–532.
[2] Hu J, Odom T, Lieber CM. Acc Chem Res 1999;32:435–45.
[3] Yogeswaran U, Chen SM. Sensors 2008;8:290–313.
[4] Anantram M, Leonard F. Rep Prog Phys 2006;69:507.
[5] Paulo A, Bokor J, Howe R, He R, Yang P, Gao D, et al. Appl Phys Lett 2005;87:053111.
[6] Sun CQ. Prog Solid State Chem 2007;35:1–159.
[7] Treacy M, Ebbesen T, Gibson J. Nature 1996;381:678.
[8] Diao J, Gall K, Dunn M. Nano Lett 2004;4:1863–7.
[9] Poncharal P, Wang ZL, Ugarte D, De Heer W. Science 1999;283:1513.
[10] Uchic M, Dimiduk D, Florando J, Nix W. Science 2004;305:986–9.
[11] Greer J, Oliver W, Nix W. Acta Mater 2005;53:1821–30.
[12] Wu X, Kulkarni J, Collins G, Petkov N, Almeicija D, Boland J, et al. Chem Mater 2008;20:5954–67.
[13] Philippe L, Peyrot I, Michler J, Hassel A, Milenkovic S. Appl Phys Lett 2007;91:111919.
[14] Ding W, Calabri L, Chen X, Kohlhaas K, Ruoff R. Comp Sci Tech 2006;66:1109–21.
[15] Sawaya S, Akita S, Nakayama Y. Appl Phys Lett 2006;89:193115.
[16] Hoffmann S, Utke I, Moser B, Michler J, Christiansen S, Schmidt V, et al. Nano Lett 2006;6:622–5.
[17] Hassel A, Rodriguez B, Milenkovic S, Schneider A. Electrochim Acta 2005;51:795–801.
[18] Supplementary Material, see Appendix A.
[19] Nanosensors. Neuchatel: Nanoworld.
[20] Taupin V, Varadhan S, Chevy J, Fressengeas C, Beaudoin A, Montagnat M, et al. Phys Rev Lett 2007;99:155507.
[21] Wu B, Heidelberg A, Boland J. Nat Mater 2005;4:525–9.
[22] Lubliner J. Plasticity theory. New York: Macmillan; 1990.
[23] FE program ABAQUS®/Standard (v 6.4).
[24] Csikor F, Motz C, Weygand D, Zaiser M, Zapperi S. Science 2007;318:251–4.
[25] Zaiser M. Adv Phys 2005;55:185.
[26] Peyrot I, Bouchard P-O, Ghisleni R, Michler J. J Mat Res 2009;24:936–47.